Chapter V. Space charge layer problems in grain boundary diffusion studies

Introduction

Space charge layer (SCL) effects are discussed in this chapter due to their importance in ionic and partly covalent materials. Unlike in materials where electrons are always available and fast, in ceramic systems there are typically two – oppositely charged – carriers the conductivity of which has to be taken into account [Duf86]. Because the individual defect formation energies differ, SCL arises and causes an electric potential difference between the surface, or GB, and the bulk interior [Leh53]. SCL affects considerably the properties of ionic materials and can in many cases be very significant [Mai95]. Despite this fact, conventional GB diffusion models typically neglect the space charge contribution. This seems to be due to two main reasons. First, the conventional models were applied historically to a large extent to metals, intermetallic compounds and alloys, in which the SCL does not exist. Preparation of ionic materials, like ceramic oxides, is much more complicated in comparison with metals and, that is why, diffusion data on these materials are still contradictory. However, nowadays one can find intensive literature on diffusion studies in oxides (for example, on diffusion in doped ZrO_2: [Kil03a], [Kil03b], [Arg04], [Tay04], [Kil04], [Tay05], on diffusion in α-Al_2O_3:

[Pro96a], [Pro96b], [Gal96], on diffusion in MgO: [Lib94], [Yoo02]). Second, it has been believed for a long time that the space charge contribution is negligible [Mis01], even at low temperatures. Indeed, the penetration profiles are treated by using Le Claire's relation for all the diffusion experiments based on penetration-depth profiles measurements without taking into account the SCLs at all. There are, however, intensive studies, e.g., in particular, on $SrTiO_3$, that show the drastic relevance of them as regard, transport [Leo99], [Gou01a].

There are several theoretical studies on discussion of the role of SCLs in diffusion studies. Yan *et al.* [Yan77] analyzed slightly enhanced diffusion near the boundaries, i.e. in the SCL, in doped and undoped KCl. Despite the fact, that this paper was not directly concerned the diffusion profiles measured by one of the appropriate techniques, Yan could suggest a model for diffusion analysis in ionic materials. Because of the SCL, the GB is to be considered as an inhomogeneous region, consisting of the GB core and the adjacent SCL. Accordingly, three diffusivities are used in Yan's model: in the bulk, SCL and GB core. The diffusivity within the SCL is suggested to be coordinate-dependent in Yan's model. Recently, Jamnik and Maier [Jam95], [Jam97a], [Jam01a] considered a similar model of the GBs in ionic materials. For this reason we distinguish here between the GB core and SCL. In this sense the GB core is the region which was supposed in the preceding chapters. The dependence of SCL diffusivity (D_{scl}) on coordinate was also taken into account in the derivations of Chung *et al.* [Chu00] on the basis of Gouy-Chapman model [Boc77]. The role of this dependence is discussed in this chapter on the basis of simulations by FEM and the program FLUX-EXPERT.

Contrary to the conclusion of Mishin and Gust on the importance of SCL [Mis01] (mostly based on the theoretical findings of Yan [Yan77]), Wang [WanR05] and De Souza [Sou05] took into account the SCL with the diffusivity different from that of the infinite bulk and surface, in order to analyze their experimental results properly. In both papers perovskite-like ABO_3 materials are concerned with SCL depleted of mobile charge carriers, *viz.* oxygen vacancies. Additionally, $SrTiO_3$ is recognized as a model electroceramic material with very different properties depending on experimental conditions [Sou03], [Mai04]. It could also be shown that SCLs can even overlap in nanocrystalline $SrTiO_3$ – the effect that we neglect in the following [Bal06]. Another important example of depleted SCL refers to ZrO_2. Here it can be mentioned that not only depth-profile measurements but also conductivity measurements provide important information on transport properties of ionic materials [Hei03]. By means of impedance spectroscopy Gou *et al.* [Gou01b], [Gou02] demonstrated the GB resistivity which was two to three orders of magnitude higher than in the bulk in yttria-doped ZrO_2 at low

temperatures. The effect was attributed to space charges and the results were successfully explained by the Mott-Schottky model [Mot39], [Scho39]. The blocking space charge effects were also observed in another fluorite structure material, namely doped nanocrystalline CeO_2 [Kim02]. The perpendicular GBs in this material lead to an additional semi-circle in the impedance spectra. The impact of those boundaries on impedance has already been discussed by Maier [Mai86]. Despite these facts, nobody has revealed the importance of SCLs adjacent to the GB cores studying oxygen in-diffusion in ZrO_2. In the following papers [Bro99b], [Knö03] on oxygen diffusion in doped and undoped nanocrystalline ZrO_2 the SCLs are completely ignored. Moreover, there are contradictions in the literature on the behavior of transport properties measured by impedance spectroscopy and depth-profiling methods [Man97], [Bro04]. Consequently, it is the purpose here to discuss the impact of SCL on diffusion in ionic materials in terms of conventional GB diffusion models.

As we are interested in fast GB transport we will focus on depletion layers between which the fast diffusing core is embedded. For simplicity's sake we again ignore the profiles within the GB core and characterize the SCL by a laterally constant effective transport coefficient. Also effects caused by electrical fields as discussed by Jamnik and Maier [Jam97b], [Jam01b] and Schmalzried *et al.* [Schm98] are neglected.

5.1 Mathematical model to describe diffusion in a polycrystal including space charge layers

Mathematically diffusion in polycrystalline materials can be described by means of differential equations, if both diffusion in the bulk and GBs obey Fick's law as it was explained in chapter I. The assumptions of an infinitely thin GB and a steplike change of the diffusion coefficient can be used for the SCL problem as well, leading to a system of three differential equations. The diffusivities are taken as time and concentration independent. The 2D case of this model suggests the following equations with C_g, C_{gb} and C_{scl} being the grain, GB and SCL concentrations, respectively

$$\begin{cases} \dfrac{\partial C_g(x,y,t)}{\partial t} = D_g\left(\dfrac{\partial^2 C_g(x,y,t)}{\partial x^2} + \dfrac{\partial^2 C_g(x,y,t)}{\partial y^2}\right) \\ \dfrac{\partial C_{scl}(x,y,t)}{\partial t} = D_{scl}\left(\dfrac{\partial^2 C_{scl}(x,y,t)}{\partial x^2} + \dfrac{\partial^2 C_{scl}(x,y,t)}{\partial y^2}\right) \\ \dfrac{\partial C_{gb}(y,t)}{\partial t} = D_{gb}\dfrac{\partial^2 C_{gb}(y,t)}{\partial y^2} + \dfrac{2D_{scl}}{\delta}\dfrac{\partial C_g(x,y,t)}{\partial x}\Bigg|_{|x|=\frac{\delta}{2}} \end{cases} \quad (5.1)$$

As usual the relevant equation in the grain is Fick's second law. The same is true for SCL as long as we ignore inhomogeneity effects and effects due to charge separation. For the GB we have to take the same form as in the Fisher system (Eq. (1.6a)). The main difference of this new model and the Fisher system is in fact, that the leakage of atoms exists from the GB to SCL. The term which controls this leakage is characterized by D_{scl}. Again, the problem is symmetrical with respect to x = 0. The relevant mathematical model corresponds to the geometrical model depicted in fig. 5.1. The thickness of SCL is denoted as δ_{scl} and is fixed to 1 nm along the calculations. The effective thickness δ_{scl} was employed in many theoretical considerations on space charges, leading to an abrupt variation of diffusion coefficients. However, there are contradictions in the literature with respect to this property. For example, in ZrO_2 δ_{scl} varies from 0.35 to 3 nm [Dij81], [Aok96]. Here the value was chosen as being the average of this range as well as from the point of view of numerical conveniences.

As before, the boundary conditions at the surface reflect a constant source and sufficiently fast surface reaction with zero initial concentration at y > 0:

$$\begin{cases} C_g(x,\ y,\ t) = C_{gb}(x,y,t) = 1 & \textbf{at}\ \ \mathbf{y\ =\ 0} \\ C_g(x,\ y,\ t) = C_{gb}(x,y,t) = 0 & \textbf{at}\ \ \mathbf{t\ =\ 0,\ y > 0} \end{cases} . \quad (5.2a)$$

The continuity conditions and mass balance were used at interfaces: between GB and SCL, SCL and grain. Correspondingly, equal fluxes and concentrations were applied:

$$\begin{cases} C_{scl}(x,y,t) = C_{gb}(x,y,t) \\ J_{scl}(x,y,t) = J_{gb}(x,y,t) \end{cases} , \quad \textbf{if}\ |\mathbf{x}| = \delta/2 \quad (5.2b)$$

and

$$\begin{cases} C_{scl}(x,y,t) = C_g(x,y,t) \\ J_{scl}(x,y,t) = J_g(x,y,t) \end{cases} \quad , \quad \textbf{if } |\mathbf{x}| = \frac{\delta}{2} + \delta_{scl}. \tag{5.2c}$$

Correspondingly, the equation describing diffusion along the GB core in Eq. (5.1) takes account of the relevant conditions at the interface between the GB and SCL (Eq. (5.2b)). The unity in Eq. (5.2a) means that the concentration is normalized with respect to the concentration at the surface. In the present study regarding the SCL problems the GB, or GB core is always assumed to represent a structurally disturbed region, i.e. we refer to the misorientation of grains. The question of the SCL to be the part of the GB or the bulk is not discussed here as it does not play a role given the above assumption. The system was numerically integrated with the flux boundary condition at the bottom of the sample used in the calculation is equal to zero (fig. 5.1). The role of this boundary condition was analyzed in the manner as discussed in chapter IV and estimated to be negligible, suggesting the obtained results correspond to the semi-infinite systems (see discussion below) and partly thin films in the sense that only the maximum of the derivative $\partial \ln C_{av}/\partial y^{6/5}$ determines D_{gb}. Importantly, all the conclusions made in chapter III are important for the SCL problems too.

The system of equations (Eq. (5.1)) was solved using FEM (FLUX-EXPERT, Simulog, France) as described in chapter II. Different kinetic regimes for different ratios of diffusivities Δ are covered, and different GB networks (parallel boundaries and square grains) are considered. In all the cases the calculated concentration distribution was numerically integrated parallel to the surface providing the average concentration (C_{av}). From the resulting concentration profiles D_{gb} values were deduced by using the conventional equations in order to compare them with the exact value (used in the simulation) and to estimate the error. In the calculations D_g and δ were fixed to $2.95 \cdot 10^{-4}$ nm^2/s ($2.95 \cdot 10^{-16}$ mm^2/s) and 0.5 nm, respectively, whereas D_{gb} and D_{scl} were varied in order to have different ratios with respect to D_g. Accordingly, the ratio $\Lambda = D_g/D_{scl}$ was introduced for convenience.

5.2 Accuracy of the simulated diffusion profiles and effect of coordinate-dependent space charge layer diffusivity

5.2.1 The finite element mesh and diffusion barrier at the bottom of the geometrical model

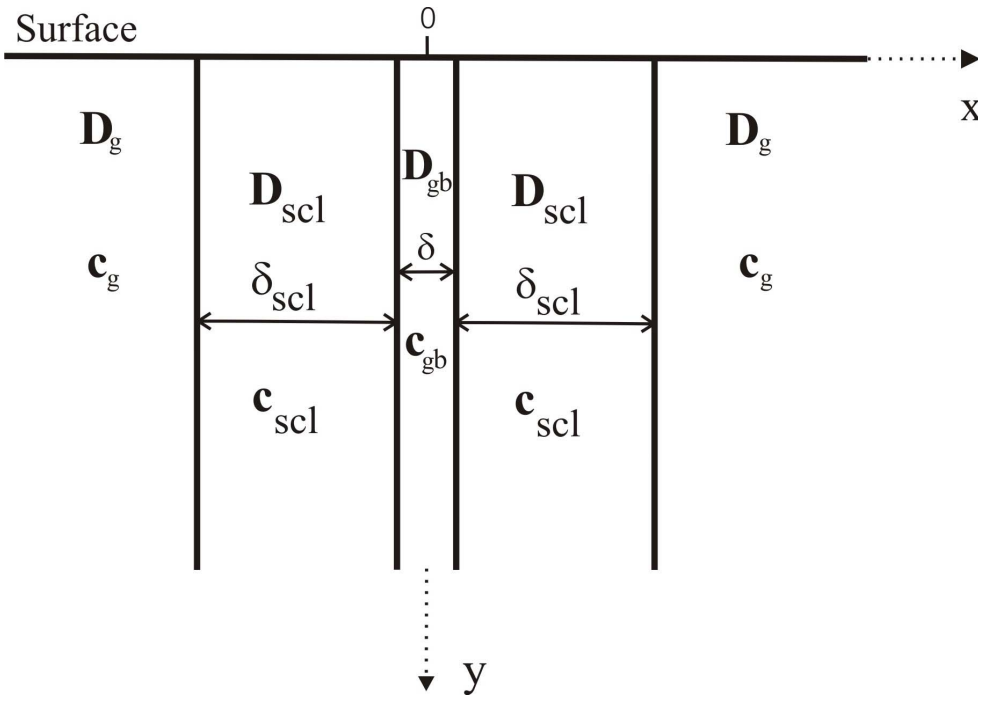

Fig. 5.1 Schematic representation of the geometrical model used for calculation including space charges.

The choice of an appropriate mesh for SCL diffusion problems is very critical due to the fact that D_{scl} differs from D_g. Different meshes (or, in other words, meshes of different densities) were tried, in order to find the most suitable one. Major emphasis was laid on optimizing the mesh in the SCL, because the problems of interest involve extremely small diffusivities in this region (blocking space charge effects). In fig. 5.2 a fragment of the mesh used for SCL diffusion is depicted. One can see a great difference between the densities of the mesh in the bulk and SCL. Such a mesh allows one to simulate diffusion in the type-B kinetics at very short t. The mesh in the SCL is homogenous as in the bulk, while close to the SCL the bulk mesh was inhomogeneous and adapted to the SCL-bulk transition. As a result, the number of triangle elements of the mesh in the SCL is about 87% of a whole number of the elements in the geometrical model (sample). However, the length of the sample was only 100 nm for simulating diffusion in the B-regime. Further increasing the mesh density did not allow D_{scl} to be more decreased, because the finite element problem with the higher density could not be solved even if the length of the sample was decreased. Consequently, the smallest value of D_{scl} used in the present study was $2.95 \cdot 10^{-7}$ nm^2/s ($2.95 \cdot 10^{-19}$ mm^2/s), and, for comparison, $D_{gb} = 2.95 \cdot 10^{-2}$ nm^2/s ($2.95 \cdot 10^{-14}$ mm^2/s). The interval between the nearest points of the mesh is about 0.03 nm and 0.5 nm in the SCL and bulk, respectively.

The mesh was also optimized for studying diffusion in the A-regime. The corresponding analysis will be given below.

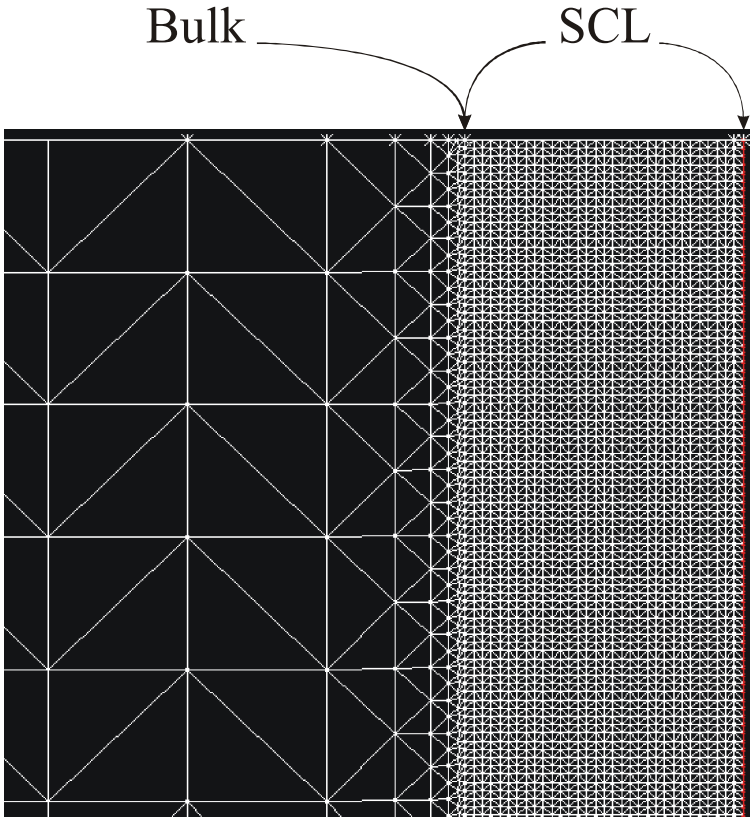

Fig. 5.2 A fragment of the mesh used to simulate diffusion in the B-regime (δ_{scl} = 1 nm). The red line represents the GB.

In order to prove that the obtained mesh is suitable for a diffusion study with various D_{scl}, the diffusion profile was calculated for the test case $D_{scl} = D_g$. This should give the same profile as obtained with mesh 1 described in chapter IV. The gradients of the corresponding profiles are compared in fig. 5.3. Obviously, there is a discrepancy between these profiles which increases along the depth indicating that the mesh density is not optimal, especially in the GB part. However, the gradients coincide at the maximum where the main interest of the present analysis lies.

Furthermore, it has to be noticed again that we are interested in small D_{scl}-values. The mesh shown in fig. 5.2 was also examined with respect to such small values. The diffusion profile was calculated for the sample comprised the SCL only in order to check the quality of the mesh. This means the bulk diffusion was simulated with the smallest D_{scl}. The corresponding diffusion profile is shown in fig. 5.4 and compared with the complementary error-function solution to diffusion equation. These profiles mostly coincide. This allowed us

to conclude that the relevant SCL mesh suffices for our purposes despite the deviations observed in fig. 5.3.

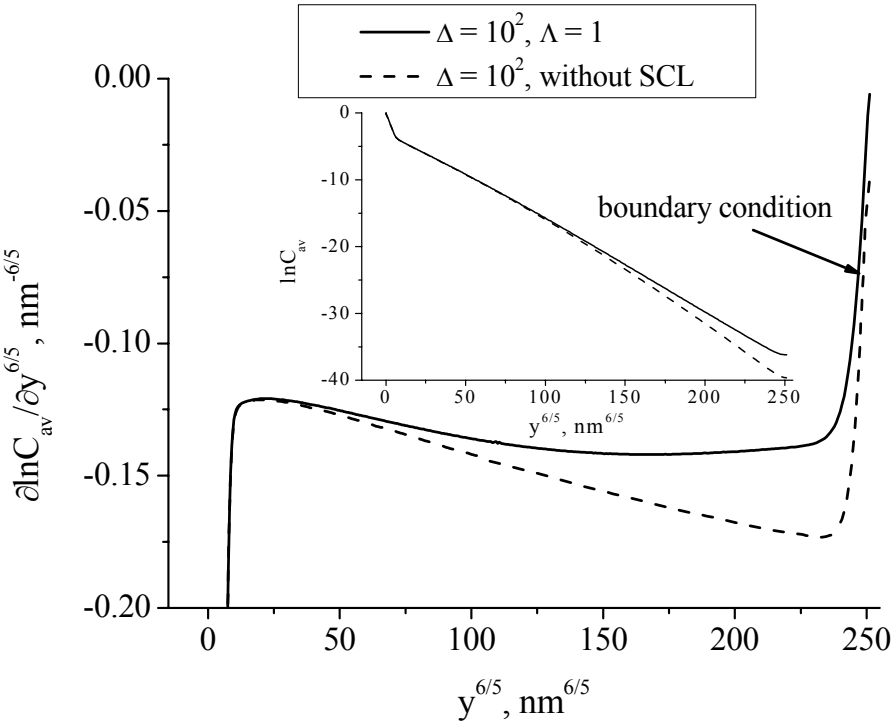

Fig. 5.3 A comparison of the mesh used for taking into account space charge effects with the mesh without the SCL having the same mesh density as for mesh 1 described in chapter IV. The profiles were calculated for the length of 100 nm at t = 4700 s. Also the $\ln C_{av} = f(y^{6/5})$ dependence is shown in inset.

Contrary to all the diffusion problems discussed so far, the meshes used for the SCL problems for simulation in the diffusion regimes of type-A and -B are very different. This is caused by extremely small diffusion lengths in the SCL under conditions of type-B kinetics. Two meshes were used to simulate the diffusion profiles in the A-regime. One mesh corresponds to simulations with $D_{scl} = 2.95 \cdot 10^{-7}$ nm^2/s and another one to values $D_{scl} = 2.95 \cdot 10^{-5}$ nm^2/s or larger. These meshes will also be analyzed with respect to the accuracy of the obtained results. In fig. 5.5 the diffusion profiles for the two values of D_{scl} are compared with the corresponding complementary error-function solutions. These calculations refer to SCL diffusion only as in fig. 5.3. The accuracy of the profile calculations is obvious, suggesting that these meshes can be used for simulating diffusion at long t. Interestingly, the density of the mesh in the SCL is 0.0625 and 0.125 for smaller and larger diffusivity, respectively. It is only double as large in the one case and four times larger in the other case

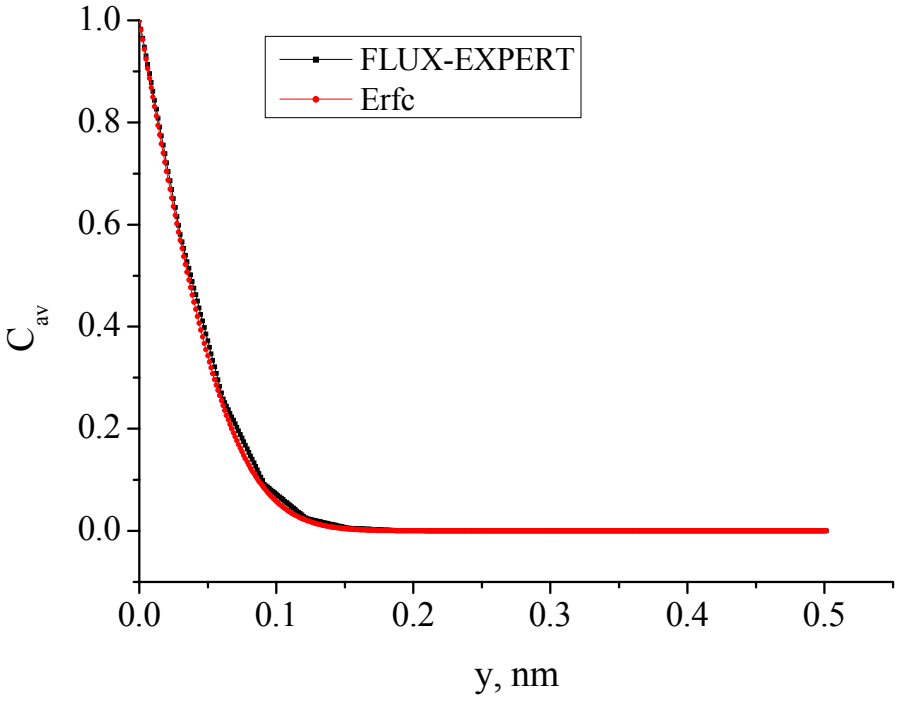

Fig. 5.4 A comparison of the bulk diffusion profiles obtained for D_{bulk} = $2.95 \cdot 10^{-7}$ nm^2/s, representing D_{scl}, with the exact analytical solution to diffusion equation given by a complementary error-function (Erfc).

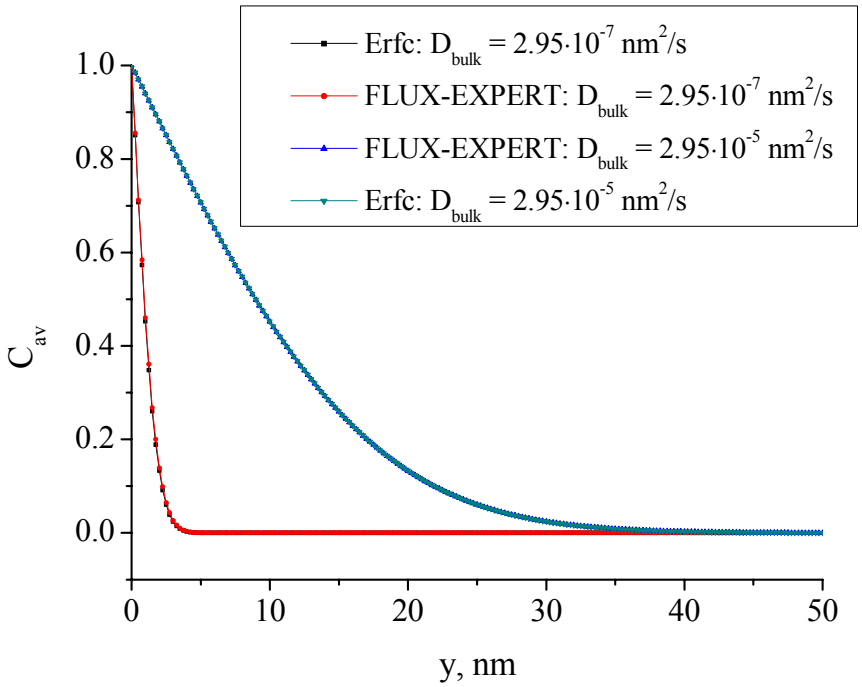

Fig. 5.5 A comparison of the two meshes (for different D_{bulk}, representing D_{scl}, see the text) used to simulate diffusion in the A-regime with the corresponding complementary error-function solutions (Erfc) at $t = 3 \cdot 10^6$ s.

as for the mesh used for the B-regime. The density of the mesh in the bulk part of the geometrical model remains unchanged and is the same as used in all the calculations in the A-regime in the present study.

One can expect that the profiles calculated for the finite element model used are affected by the boundary condition at the bottom of the sample (geometrical model). This indeed plays an important role when simulating diffusion along the GBs accompanied by diffusion in the SCL with very small D_{scl}. Accordingly, one can plot the derivative of the profile calculated for the smallest D_{scl}. In fig. 5.6 such a derivative is shown (solid curve). As it was explained in chapter IV, the strong effect of the boundary condition is reflected in the extreme case that the maximum of the profile disappears, because the gradient goes to zero. This refers to the question of validity of the solutions for semi-infinite systems for the problem discussed here. As it is seen in fig. 5.6 the maximum is very well distinguishable and can be very easily estimated. The rest of the profile is affected by different factors, including the zero flux condition at the bottom. This also indicates that a sample length of 100 nm can be used to simulate diffusion in the B-regime.

5.2.2 The reason of using constant space charge diffusivity

First, it should be again noted that the main interest is related to the maximum of the derivative of the diffusion profile. This maximum gives the proper value of D_{gb} when deduced by using the conventional Le Claire relation. The constant D_{scl} used in the present simulation is questionable, since the concentration of defects varies with the distance perpendicular to the GB. That is why, for example, Chung *et al.* [Chu00] proposed the model of diffusion along the GBs with the adjacent SCLs based on the Gouy-Chapman model, in which D_{scl} is coordinate dependent. In order to check the effect of the coordinate dependent D_{scl}, the SCL thickness (δ_{scl}) was drastically reduced and a new model was developed.

Decreasing δ_{scl} from 1 nm to 0.03 nm, the SCL thickness was reduced to an unrealistically and infinitely thin region. However, the effect of blocking SCL is so strong, that the position of the maximum of the derivative is very similar to that for δ_{scl} = 1 nm as fig. 5.6 shows. The values of the derivatives are also very close, suggesting that the maximum is determined by what happens in the first atomic layers close the GB core independent of thickness of the SCL and dependence of the diffusivity on coordinate. This means, that the maximum reflects directly the movement of the atoms from the GB core into the SCL. It is the same as the B-regime starts immediately when the leakage of diffusing atoms starts from

the GB into the grain. The beginning of this process determines the position of the maximum and its magnitude. To investigate further the insensitivity of the maximum on the coordinate dependence of D_{scl}, an additional calculation was performed. In the new calculation δ_{scl} was increased to 3 nm, and the SCL itself was divided into three regions with the thickness of 1 nm each. The diffusivities were different in all the three regions and varied from $2.95 \cdot 10^{-7}$ nm^2/s in the first region directly adjacent to the GB core to $2.95 \cdot 10^{-5}$ nm^2/s in the third region followed by the bulk (fig. 5.8). The concentration is enhanced in the first region due to the leakage from the GB core. This region is mostly filled by the diffusant at sufficiently long t such that it can lead to the flux of atoms to the second region. Interestingly, there is no leakage from the third region to the second one. The diffusion profiles calculated in this model are compared with those with the constant D_{scl} (δ_{scl} = 1 nm) at different t in fig. 5.7. There is no significant difference between the two models, indicating the overall result is determined by the region adjacent to the GB core even at long t. At shorter t the rest of the diffusion profiles becomes much more different depending on δ_{scl} and coordinate dependent D_{scl} (not shown here). Importantly, the maximum is not affected remaining the same under these quite different conditions. The fact that the diffusion profiles have two distinguishable parts at $t = 3 \cdot 10^6$ s will be discussed in the coming section.

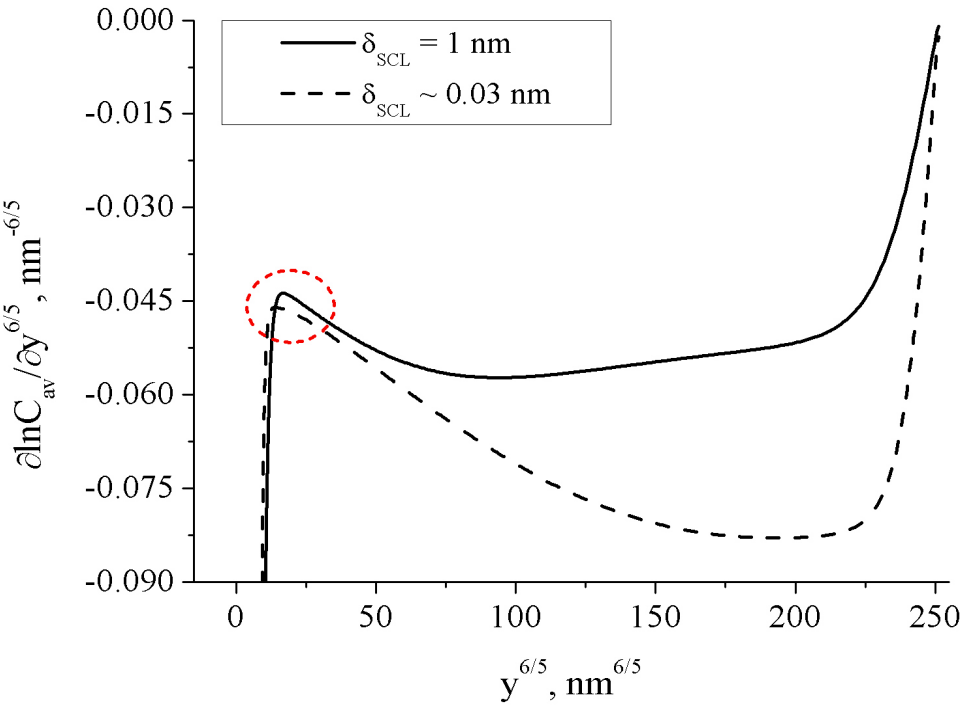

Fig. 5.6 Variation of the derivative $\partial \ln C_{av}/\partial y^{6/5}$ with $y^{6/5}$ calculated for two different SCL thicknesses for $\Delta = 10^2$.

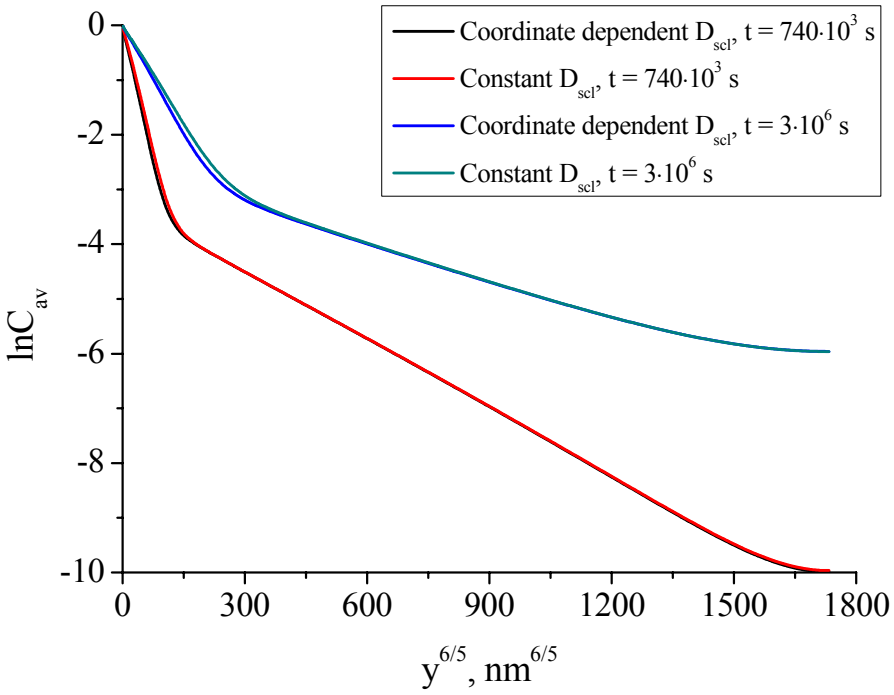

Fig. 5.7 Variation of $\ln C_{av}$ with $y^{6/5}$ calculated for the cases of constant and coordinate dependent D_{scl} for $\Delta = 10^2$.

5.3 How diffusion proceeds in the models of parallel boundaries and square grains

Two models were used to study diffusion in ionic materials, namely the model of parallel boundaries (or, isolated GB model, if $L_g < d/2$) and of square grains. As it was explained in chapter IV, these are the most important models, allowing diffusion to be characterized even in realistic polycrystalline microstructures. As usual, t and d were taken quite small, in order to reproduce situations in nanocrystalline materials. Emphasis is laid on the blocking effect recently observed in variety of ionic materials [see, for example, [Gou02]]. Consequently, the SCL diffusivities (D_{scl}) are supposed to be smaller than the grain diffusivities (D_g), whereas the GB diffusivity (D_{gb}) exceeds both. However, the situations when $D_{scl} > D_g$ are also discussed in order to analyze the whole trend of the ratio $D_{gb,app}/D_{gb,true}$ (here $D_{gb,app}$ is, as usual, an apparent GB diffusivity found by applying conventional models, and $D_{gb,true}$ is a true GB diffusivity used to simulate the diffusion profiles) as a function of $\Lambda = D_g/D_{scl}$. The latter is a new parameter which makes the analysis simpler. For both models and different diffusion regimes a recipe is given how to properly

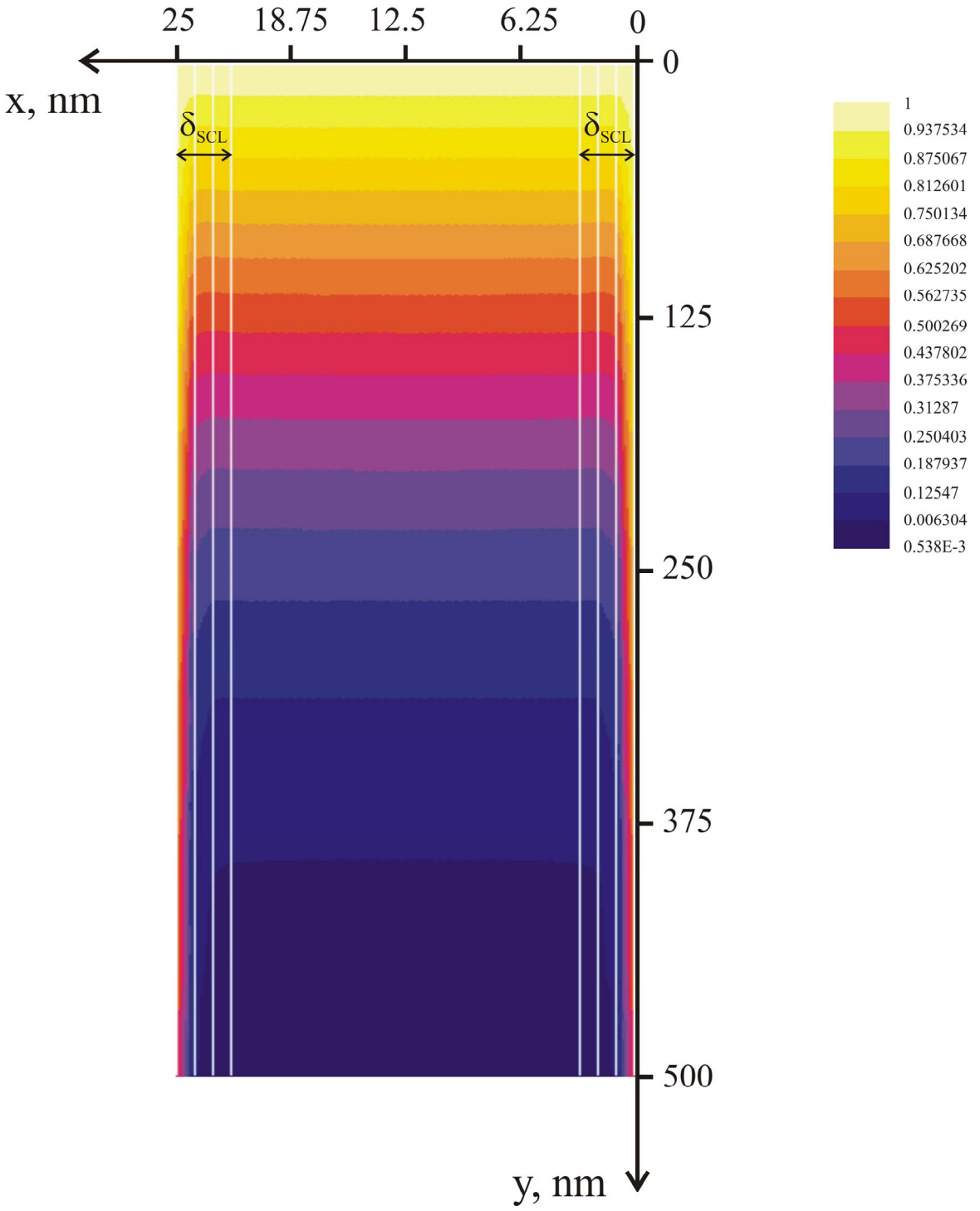

Fig. 5.8 Concentration distribution in the model of parallel boundaries with the SCL of the thickness 3 nm, comprising three parts with different diffusivities. The free surface is at y = 0 nm, whereas two neighboring parallel boundaries are at x = 0 and 25 nm, respectively. The result was obtained under conditions of the conventional A-regime, i.e. L_g is larger than the distance between the parallel boundaries. White lines show the borders of corresponding regions of different diffusivities. There is no a special physical property along white lines. Each color corresponds to certain value of the concentration, what is explained on a color pattern.

find D_{gb}. The suggestions which can be found in this chapter supplement the observations of the preceding chapters. Consequently, the problems of Le Claire's constant and the nonlinearity are also relevant here.

5.3.1 The model of parallel boundaries under conditions of type-B kinetics

It is important to note once more that both the model of parallel boundaries and the isolated GB model lead to the same results until $L_g > d/2$, where d is the average grain size or the distance between two neighboring parallel boundaries. In the present study for ionic materials the isolated GB model was used (what is caused by a very dense mesh used in the SCL) at extremely short t. Thus, only diffusion in the B-regime occurs. Consequently, the obtained results are valid for parallel boundaries as well. Trying various values for D_{scl} the diffusion profiles were calculated for fixed D_g (= $2.95 \cdot 10^{-4}$ nm^2/s) and D_{gb} (= $2.95 \cdot 10^{-2}$ nm^2/s). In fig. 5.9 the profiles are presented, with Λ (= D_g/D_{scl}) varying from 10^{-1} to 10^3. According to the conventional procedure, the profiles represent dependences in the form $\ln C_{av} = f(y^{6/5})$. The smallest value of D_{scl} is $2.95 \cdot 10^{-7}$ nm^2/s, which corresponds to the diffusion length in the SCL $3.73 \cdot 10^{-2}$ nm at t = 4700 s. Such a value scales with the density of mesh used to simulate diffusion in the SCL, what also confirms the quality of obtained result. Additionally, a very small value of D_{scl} would mean a very small contribution of diffusion in the SCL. However, the slopes of diffusion profiles vary with Λ (fig. 5.9) which is usually unknown in the experiments. This is why, it became particularly important to estimate the errors of determining D_{gb} introduced by the SCL using the conventional procedures.

As one can see in fig. 5.9, the slope decreases as Λ increases, or as D_{scl} becomes smaller. The profile for $\Lambda = 1$ is also shown in fig. 5.9 and, it is possible, at least qualitatively, to state that D_{gb} found from such profiles by applying the Le Claire relation is overestimated, if $\Lambda > 1$. On the other hand, the slopes of the profiles calculated for $\Lambda < 1$ increase, what leads to opposite trend in the $D_{gb,app}$ behavior. Because of these two trends, one has to distinguish diffusion under different conditions: $\Lambda < 1$ or $\Lambda > 1$. The purpose of this distinction is to emphasize different physical situations, but the procedure to deduce D_{gb} is the same. The difference between the two situations is demonstrated in fig. 5.10. In this figure fragments of the concentration fields are shown at t = 4700 s. If $\Lambda > 1$, diffusion is prolonged in the bulk and along the GB core, and one can immediately see, that there are fluxes from the GB core to the SCL and from the grain (bulk) to the SCL. The concentration field around the GB core is exactly what is expected for the non-overlapping fluxes from the neighboring parallel

diffusion paths. Such a contribution of the SCL is also similar to the situation, when diffusing atoms cannot move inside the material from the source due to the surface reaction, but because of the fast surface diffusion the atoms move along the surface (or along the GB core, if it is concerned). The blocking effect is reflected by the drastically reduced concentration within the SCL, and the question arises how this can affect the diffusion profile. Contrary, there is a flux from the SCL into the grain, if $\Lambda < 1$ (fig. 5.10b). Here the question about the overlapping within the SCL is not relevant, and the SCL can be filled by the diffusant in a very short time. It looks like the GB has increased its thickness due to the SCL, especially at higher diffusion times. However, it is also a matter of parameters, like the thickness δ_{scl} and diffusivity D_{gb}. It can be mentioned, that the overall process is not prolonged under conditions of $\Lambda < 1$. This is clear, as prolongation is only caused by great difference in the diffusivities in the two adjacent regions. Such a prolongation is more typical for diffusion for $\Lambda > 1$. One can see that the isoconcentration lines in fig. 5.10a are almost parallel to the GB core, i.e. the angle between them is very small – a situation typical for large values β and short t.

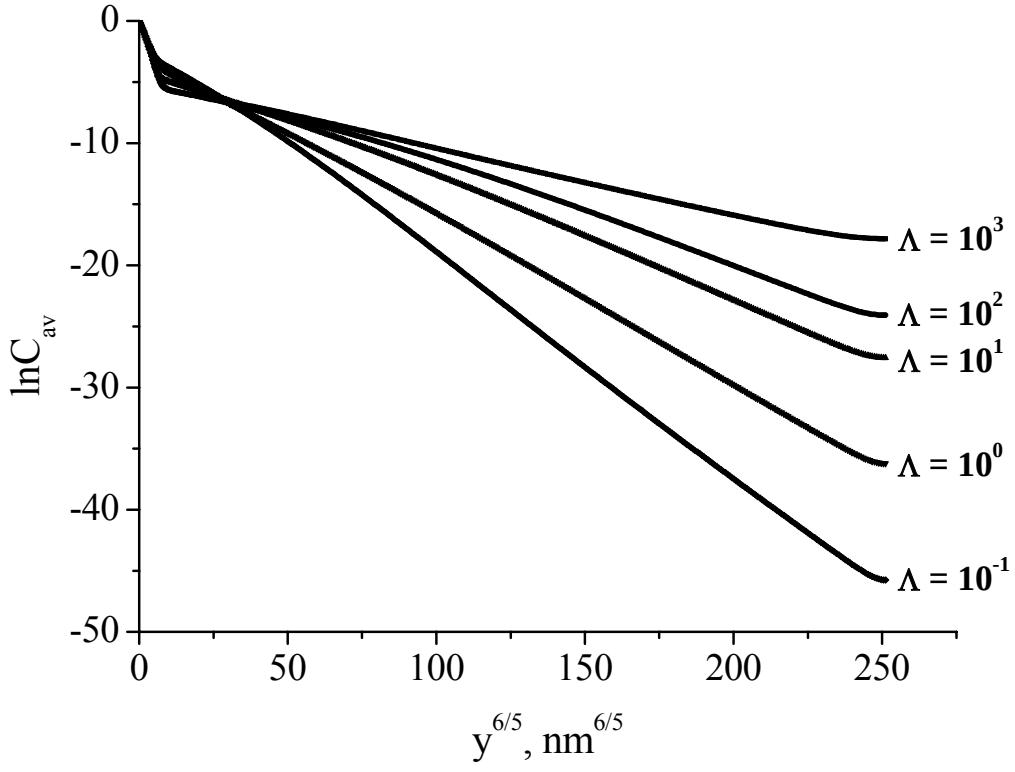

Fig. 5.9 Variation of $\ln C_{av}$ with $y^{6/5}$ calculated at t = 4700 s for $\Delta = 10^2$ and various Λ.

a)

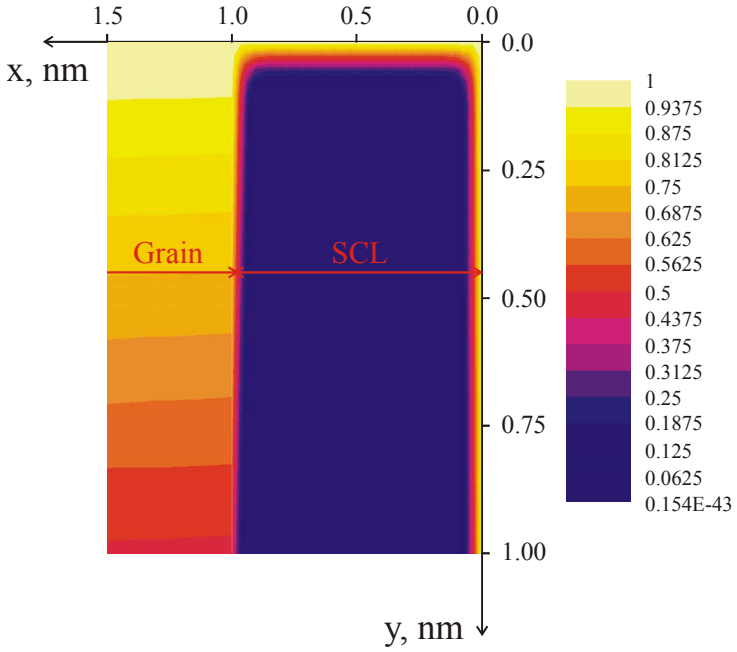

b)

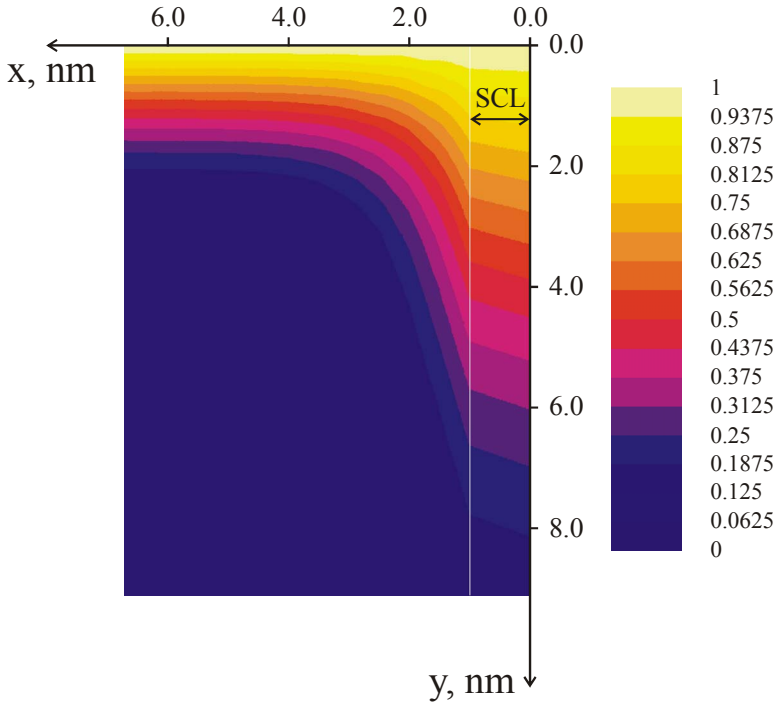

Fig. 5.10 A fragment of the concentration distribution in the model of isolated GB (the GB core is sitting exactly at x = 0 nm) with the adjacent SCL of the thickness 1 nm. As usual, a free surface is situated at y = 0 nm. Parameters: a) $\Lambda = 10^3$, $\Delta = 10^2$, t = 4700 s and b) $\Lambda = 10^{-1}$, $\Delta = 10^2$, t = 4700 s. The color patterns have their usual meaning.

The errors of using Le Claire's relation are demonstrated in fig. 5.11. Three curves are shown corresponding to three different procedures of deducing D_{gb}. First, $D_{gb,app}$ was calculated by using the standard Le Claire relation with a constant of 1.322 (Eq. (1.16)). The corresponding errors are shown as circles in fig. 5.11. This means that fitting the calculated diffusion profiles to the straight line was applied. In this case $D_{gb,app}$ is larger than the true one by a factor of about 3 at $\Lambda = 10^3$. Then the maximum of the derivative $\partial \ln C_{av}/\partial y^{6/5}$ was taken and used in Le Claire's relation (squares in fig. 5.11). In chapter III it was shown that this maximum gives the more accurate value for D_{gb} when Le Claire's relation is used. Taking the maximum leads to even larger errors in comparison with the errors of the standard fit, and D_{gb} is overestimated by a factor of 4 at $\Lambda = 10^3$. Moreover, the ratio $D_{gb,app}/D_{gb,true}$ is not unity at $\Lambda = 1$ in both cases. Obviously, this is related to the constant of 1.322. According to the findings of chapter III, the derivative $\partial \ln C_{av}/\partial w^{6/5}$ should be calculated properly depending on the parameter α ($=\delta/2L_g$). Finally, the improved derivative $\partial \ln C_{av}/\partial w^{6/5}$ was calculated by using Eq. (2.1) and put into the original Le Claire relation (Eq. (1.14)) instead of the constant 1.322. The latter is caused by very short t involved in the simulation, and all the discussions of chapter III are relevant here too. The parameter α is about 0.21 at t = 4700 s for $D_g = 2.95 \cdot 10^{-4}$ nm^2/s. Following this improved procedure, the ratio $D_{gb,app}/D_{gb,true}$ was recalculated and finally achieved unity at $\Lambda = 1$ (triangles in fig. 5.11). But, the errors in finding D_{gb} increase further even after applying the improved procedures, giving D_{gb} overestimated by a factor of about 6 at $\Lambda = 10^3$. Interestingly, the attempts to reduce the errors by using the improved procedures make the discrepancy between the apparent and true diffusivities larger. This is related to the fact that the equations used for calculating D_{gb} completely ignore the third diffusivity involved in the process, namely D_{scl}. One has to pay attention that the flux of atoms moving from the GB core into the SCL is determined by D_{scl} and, therefore, the maximum of the derivative as being determined by this motion, should reveal something close to the ratio of diffusivities D_{gb}/D_{scl}. This ratio is obviously larger than Δ and Λ for the blocking SCL, because $D_g > D_{scl}$. However, this expectation should be clarified.

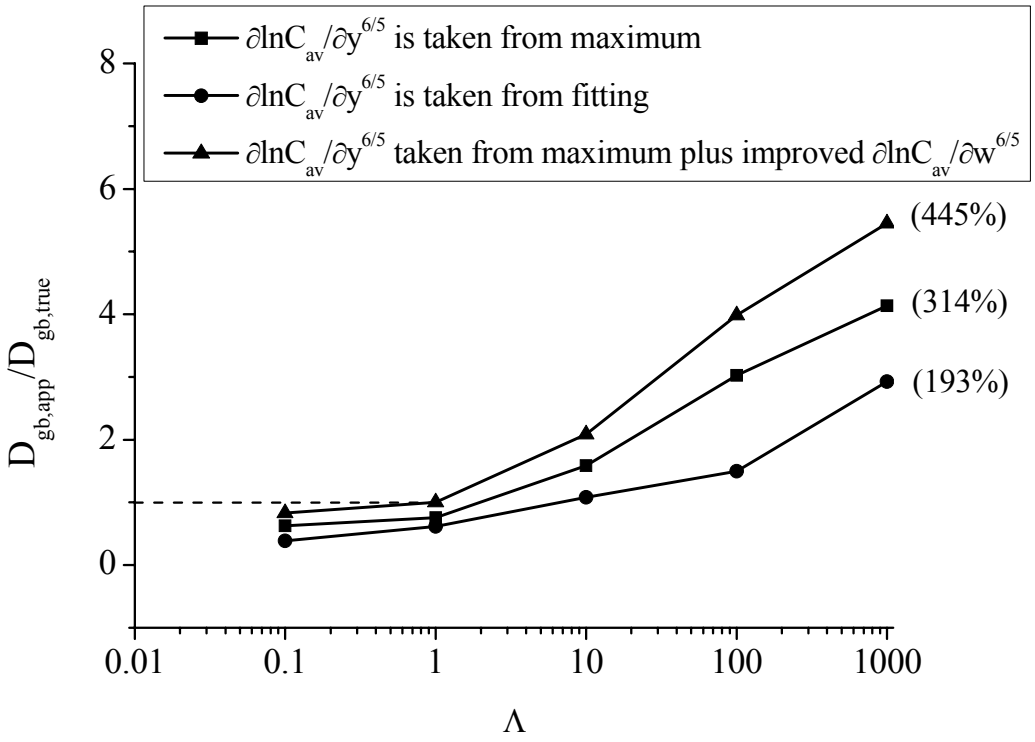

Fig. 5.11 Errors in calculating D_{gb} by using the conventional Le Claire equation and the improved procedures discussed in chapter III. The calculated profiles correspond to $\Delta = 10^2$ and t = 4700 s. Errors were estimated according to $\left(\left|D_{gb,app} - D_{gb,true}\right| / D_{gb,true}\right) \cdot 100\%$.

The blocking SCLs are accompanied by two processes. One is related to diffusion from the GB core into the SCL and another one is related to diffusion from the grain into the SCL. These processes are taken into account by the continuity conditions at the corresponding interfaces (Eq. (5.2a) and (5.2b)). In order to clarify, which process really determines the maximum of the derivatives, the plots $\partial \ln C_{av}/\partial y^{6/5} = f(y^{6/5})$ were analyzed and the equations derived in chapter III applied. The corresponding maxima for the SCL problem are rather small (fig. 5.12) and comparable to those in figs. 3.8a or 3.8b, i.e. for non-space-charge problems with $\Delta = 10^2$ or 10^3. However, the calculations differ by values of the diffusivities in the region adjacent to the GB core (i.e., D_g for the results in fig. 3.8 and D_{scl} in fig. 5.12). For $\Lambda = 10^3$ and $D_{scl} = 2.95 \cdot 10^{-7}$ nm^2/s the ratio D_{gb}/D_{scl} equals 10^5. The same ratio was realized in chapter III with $D_g = 2.95 \cdot 10^{-4}$ nm^2/s and $D_{gb} = 2.95 \cdot 10^{1}$ nm^2/s. However, the values of the corresponding maxima differ by two orders of magnitude. Generally, increasing Δ with fixed D_g leads to smaller values of the maxima. But, increasing Δ (=D_{gb}/D_{scl} for the SCL problem) with fixed D_{gb} leads to much smaller deviations in the derivatives for different ratios in

comparison with the results in fig. 3.8, from -0.12 for $\Lambda = 10^0$ ($D_{gb}/D_{scl} = 10^2$) to -0.04 for $\Lambda = 10^3$ ($D_{gb}/D_{scl} = 10^5$). Probably, the latter effect depends on the absolute value of D_{scl}. It is difficult to expect the ratio between the diffusivities knowing only the absolute value of the derivative at the maximum. A new procedure should be used in order to extract this ratio. Moreover, in the SCL problems a third diffusivity is involved (D_{scl}) which is also unknown. However, this diffusivity determines the value of the maximum.

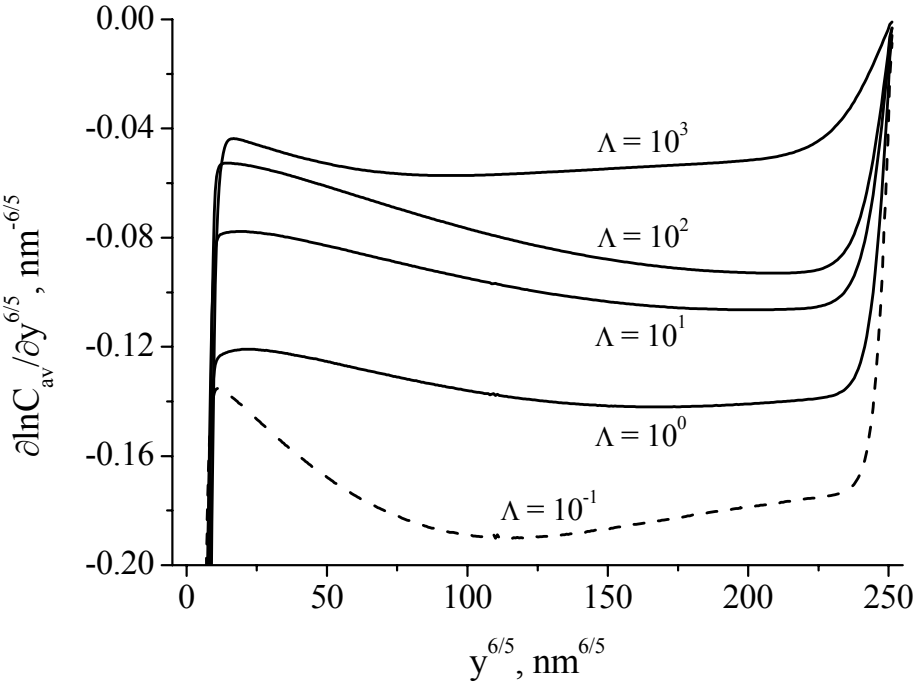

Fig. 5.12 Variation of the derivative at t = 4700 s for $\Delta = 10^2$.

In fig. 5.13 the derivatives are compared with the results of Whipple's solution integration (Eq. (1.9a)) which were obtained by fixing D_{gb} and varying D_g and D_{scl}, respectively. In the integration the same ratios of diffusivities were used as for the SCL problem, i.e. Δ in the integration equals D_{gb}/D_{scl} in the simulation (Δ in fig. 5.13 indicates the ratio used in the simulation). One can easily see that the derivatives simulated for the SCL problem are very close to those obtained by the integration, despite the fact that there is a flux of atoms from the grain into the SCL. This confirms that the maximum of the derivative is determined mostly by what happens between the GB core and the SCL. In fig. 5.13 the positions of maxima of the SCL problem slightly differ in comparison with Whipple's solution integration. The maximum is shifted to larger values of $y^{6/5}$ in the case of the SCL problem (red curves), especially for larger Λ.

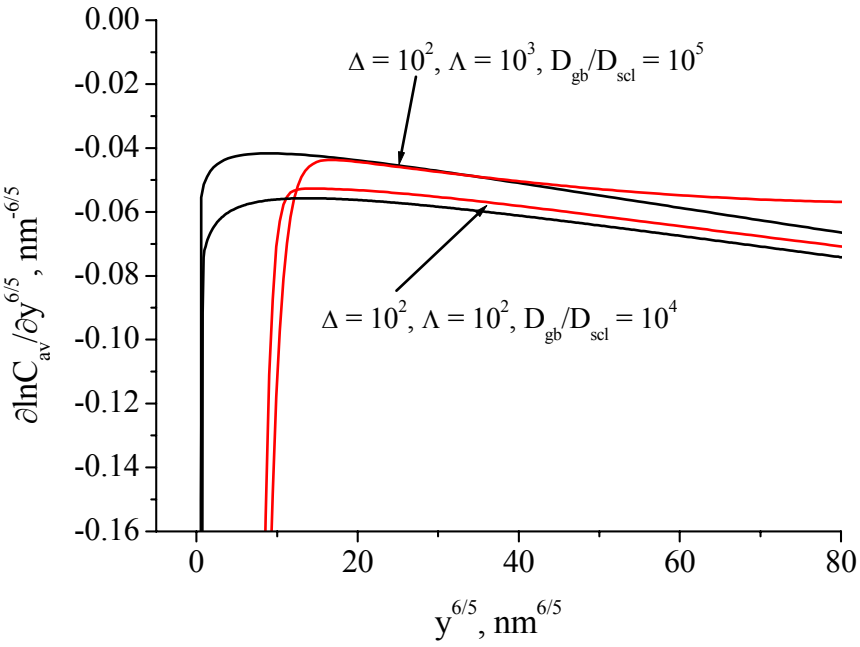

Fig. 5.13 A comparison of Whipple's solution and the simulation result of the SCL problem at t = 4700 s. The black curves correspond to Whipple's solution, whereas the red curves are responsible for the simulation.

Interestingly, the contribution of bulk diffusion can be observed at very short t. In fig. 5.14 different profiles simulated for the SCL problem are compared, and the complementary error-function solution is shown for D_g. The bulk diffusion is responsible for the process in the near-surface part of the profile for the smaller D_{scl}. However, this contribution becomes less pronounced, if Λ decreases. It means that, in principle, D_g can be still extracted even for blocking SCL, how it is done in the experiments [Sou05]. The bulk diffusion part is quite short and is followed by the part determined by the ratio D_{gb}/D_{scl}. Since D_g is smaller than D_{gb}, the process along the GB in the blocking SCL problem is characterized by even smaller slopes that one could expect to give a larger diffusivity. It should also be noticed that the profiles in fig. 5.14 are intersecting at $y^{6/5} \approx 30$ nm$^{6/5}$. For $y^{6/5} < 30$ nm$^{6/5}$ the area under these curves or the total amount of material entering the sample is larger for the smallest ratio Λ = 0.1. For $y^{6/5} > 30$ nm$^{6/5}$ the opposite situation is observed. Nevertheless, it was found out that in the whole range of $y^{6/5}$ the total area is increased for Λ = 0.1. Consequently, the blocking SCLs decrease the total amount of material in the sample, at least at short t.

In order to improve the determination of D_{gb}, the new equation, discussed in chapter III (Eq. (3.7)), was used instead of Le Claire's relation. This equation relates the maximum of

the derivative $\partial \ln C_{av}/\partial y^{6/5}$ and the ratio Δ, or specifically for the SCL problem, the ratio D_{gb}/D_{scl}. Thus, Eq. (3.7) can be rewritten in the following form

$$\left|\frac{\partial \ln C_{av}}{\partial y^{6/5}}\right|_{max} = C \cdot \left(\frac{D_{gb}}{D_{scl}}\right)^{F} \cdot t^{B}. \tag{5.3}$$

One of the ideas which can automatically arise is the fitting experimental data to Eq. (5.3). However, this equation cannot be used for real fitting, since consisting of two multiplied unknown parameters, i.e. C and Δ^F (here Δ means the ratio D_{gb}/D_{scl} as well). By using the fitting one can only find the prefactor to t^B, i.e. the whole term $C(D_{gb}/D_{scl})^F$. So the application of this equation requires knowledge of the unknowns C, F and B. As it was mentioned in chapter III the unknown parameter C is dependent on D_g and can strongly vary. Because of the problem of fitting, these parameters were estimated by integrating Whipple's solution for the diffusivities used to simulate diffusion for the SCL problem. The results are summarized in table 5.1. The integration was performed fixing D_{scl} and varying D_{gb}, i.e. to guarantee D_{gb}/D_{scl} to be 10^2 and 10^5 in order to have extremely different ratios. For each ratio D_{gb}/D_{scl} two very different t were realized, namely $2\cdot10^3$ s and 10^6 s, providing the quantities B, C and F. Consequently, this procedure was applied for each D_{scl} and Λ used. The absolute value of B slightly decreases with increasing Λ, C varies significantly with Λ, whereas F remains constant. The apparent GB diffusivity ($D_{gb,app}$) was calculated according to

$$D_{gb,app} = \frac{4}{\left(D_{gb}/D_{scl}\right) t\delta^2}\left(-\frac{\partial \ln C_{av}}{\partial w^{6/5}}\right)^{10/3}\left(-\frac{\partial \ln C_{av}}{\partial y^{6/5}}\right)^{-10/3}, \tag{5.4}$$

where the ratio D_{gb}/D_{scl} is known from Eq. (5.3) and the derivative $\partial \ln C_{av}/\partial w^{6/5}$ is found according to the improved procedure . The errors in finding D_{gb} were decreased by applying Eqs. (5.3) and (5.4) in comparison with Le Claire's relation (table 5.1). Still remaining errors can be attributed to deviations of the corresponding maxima from the result of integration of Whipple's solution (fig. 5.13). Consequently, Eq. (5.4) may be used to find $D_{gb,app}$. The disadvantage of this relation is in fact that it requires knowledge of all the parameters involved: C, B, F. Here a hint can be given for future research. It is particularly important to find a procedure to deduce D_{gb} in ionic materials. Eq. (5.3) seems to be a suitable candidate to improve the determination of D_{gb}. Further evaluations using Whipple's solution could help to correlate the maxima and ratios and all the other parameters.

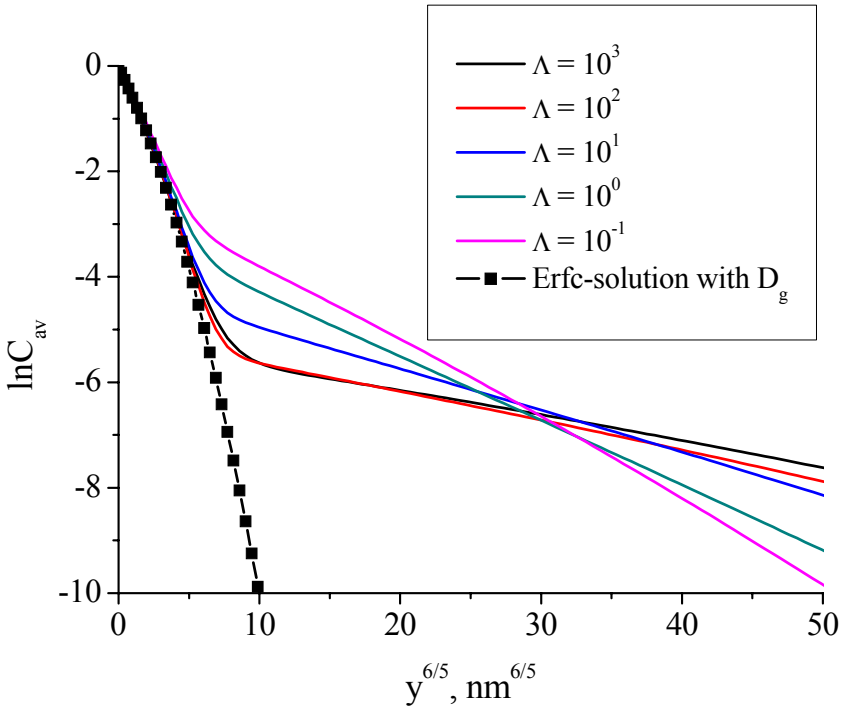

Fig. 5.14 A comparison of the profiles for different Λ and a complementary error function solution (Erfc-solution) in the region of very small depths.

Table 5.1 The parameters obtained to evaluate Eq. (5.3) and apparent GB diffusivities found by using Eq. (5.4) for t = 4700 s. As usual the errors were found due to $\left(\left|D_{gb,app} - D_{gb,true}\right| / D_{gb,true}\right)\cdot 100\%$.

Λ	B	C	F	$D_{gb,app}$, nm^2/s	Error in %
10^3	-0.47	2540	-0.61	$9.11\cdot10^{-4}$	97
10^2	-0.43	562.65	-0.60	$4.03\cdot10^{-3}$	86
10^1	-0.38	134	-0.60	$1.09\cdot10^{-2}$	63

5.3.2 The model of square grains under conditions of type-B kinetics

The model of square grains was used here to analyze the effect of blocking GBs under realistic conditions. The results obtained for this model with space charge effects included were compared with those obtained for the model of parallel boundaries and the model of square grains without SCLs. The importance of blocking SCLs lies in the channeling of transport. In other words, the reduced diffusivities in the regions adjacent to the GBs suggest an enhanced β-parameter (Eq. (1.9d)) and, as a result of this, increased penetrations. Indeed, the increased ratios between the diffusivities lead to smaller slopes, as it was shown in the

preceding section (fig. 5.12). If the perpendicular GB comes into play, the slope is changed the more strongly, the shorter diffusion time or the larger ratio between the diffusivities. The profile calculated for $\Lambda = 10^2$ and $\Delta = 10^2$ for the model of square grains is compared with that for the model of parallel boundaries and square grain without the SCL (fig. 5.15a). Because the ratio of diffusivities Δ is small, there are no corresponding contributions of perpendicular GBs in the model of square grains without SCL (see, for example, fig. 4.9). This makes the profile for the square grains without the SCL very comparable to the profile for the parallel boundaries without SCLs. Despite such a role of perpendicular GBs for the small ratio Δ, the slopes of the profiles for the square grains with the SCL are very different in comparison with the slopes of those profiles obtained without the SCL. Consequently, the role of GBs surrounded by the blocking SCLs is very specific and important. Moreover, the slope of the profile with the SCL decreases with Λ. It can make $D_{gb,app}$ larger applying the conventional equations, whereas the slope is increased in the problems without the SCL (fig. 4.9). This, obviously, yields one more specific role of the blocking SCL. Some diffusion profiles were also calculated for larger Δ. According to fig. 5.15b the contribution of perpendicular GBs is reflected in the larger slope in comparison with the situation when only parallel boundaries contribute. It is very clearly seen in fig. 5.15b that the slope of the profile is decreased by the influence of the blocking SCLs. Because the effects in the problems with and without the SCLs have opposite trends in the slope behavior, the question is only which of them dominates. In the case of the SCL problems, the contribution is directly determined by the ratio Λ. Obviously, the larger Λ, the smaller the slope. Since the results in figs. 5.15a and 5.15b have the same Λ, these are also comparable. The profile for larger Δ is characterized by typical spikes which are very tiny in comparison with the profiles without the SCLs. Surely, this is due to diffusion confined within the GBs in the SCL problem, i.e. there is no significant diffusion from the GBs to the adjacent SCLs.

5.3.3 The model of parallel boundaries and the model of square grains under conditions of type-A kinetics

According to fig. 1.5 the increase of t should finally lead to the A-regime. As far as the overall process is determined to a great extent by the ratio of the GB and SCL diffusivities, the A-regime is met when the diffusion length in the SCL is comparable to that in the grain and GB. It can be understood in the way that three different processes should have similar diffusion lengths, leading to a homogeneous situation. If this is not the case, and the processes

are still separable, the homogeneous solutions, such as Hart' equation (Eq. (1.17a)) lead to significant errors. The diffusion time needed to reach the homogenous situation can be extremely long, giving unrealistic values of several tens of millions seconds. In order to emphasize these points, the concentration distribution is shown in the model of parallel boundaries in fig. 5.16 at $t = 3 \cdot 10^6$ s for $\Lambda = 10^3$. At such a high t nominally the A-regime is valid, as being determined by the condition $L_g > d$ ($L_g \approx 30$ nm, $d = 25$ nm). In the region of SCL the concentration differs from that in the bulk. The contribution from GBs enhances the concentration within the SCL at high t despite a very small diffusivity D_{scl}. The role of SCLs is not the same as it was at short t. The contribution to the grain comes partly from the combined SCL-GB system. In this sense both the regions, the SCL and GB, represent one part of the sample. This is similar to what was discussed in section 5.2.2. Because of the blocking effect, first, some time is needed to fill the SCL by the diffusant, and then the contribution would continue from the SCL-GB into the grain. As a result, the diffusion profiles obtained under the nominal A-regime conditions comprise two distinguishable parts. In fig. 5.17 the diffusion profile calculated for the model of parallel boundaries with the SCL at high t is compared with that without SCL. Two interesting cases are also compared in fig. 5.17, namely $\Lambda = 10$ and $\Lambda = 10^3$. If the ratio Λ is small enough, the corresponding profile strongly differs from that for larger Λ and is close to the profile without the SCL, also shown fig. 5.17. The latter difference arises at very low concentrations due to the changed kinetics. However, if the larger Λ occurs, the two parts of the profile arise. Consequently, it would be necessary to apply the conventional procedure used for the B-regime. On the other hand, the A-regime is relevant. The problem, of course, deals with the conditions (Eqs. (1.9), (1.10), (1.11)) which do not take into account the third diffusivity involved in the process. The Hart equation, being the equation for the A-regime, was used to find $D_{gb,app}$, and the errors were indeed observed (fig. 5.18). The errors in finding D_{gb} are high, suggesting that it is underestimated, if the conventional equation is used. The error increases with Λ, reaching 88% at $\Lambda = 10^3$. The shorter t the larger the error (in the A-regime). For $\Lambda = 10^2$, $t = 50 \cdot 10^6$ s is sufficient to reach the ratio $D_{gb,app}/D_{gb,true} \approx 1$. On the other hand, applying Le Claire's relation gives even larger error. Because the profile with the two distinguishable parts is observed for large Λ, the procedure discussed in the preceding section can be applied, if one believes that the slope of the profile reflects the process between the GB and the SCL at $t = 3 \cdot 10^6$ s. Accordingly, the quantities B, C and F were taken from table 5.1 for $\Lambda = 10^3$ and Eqs. (5.3) and (5.4) were used

a)

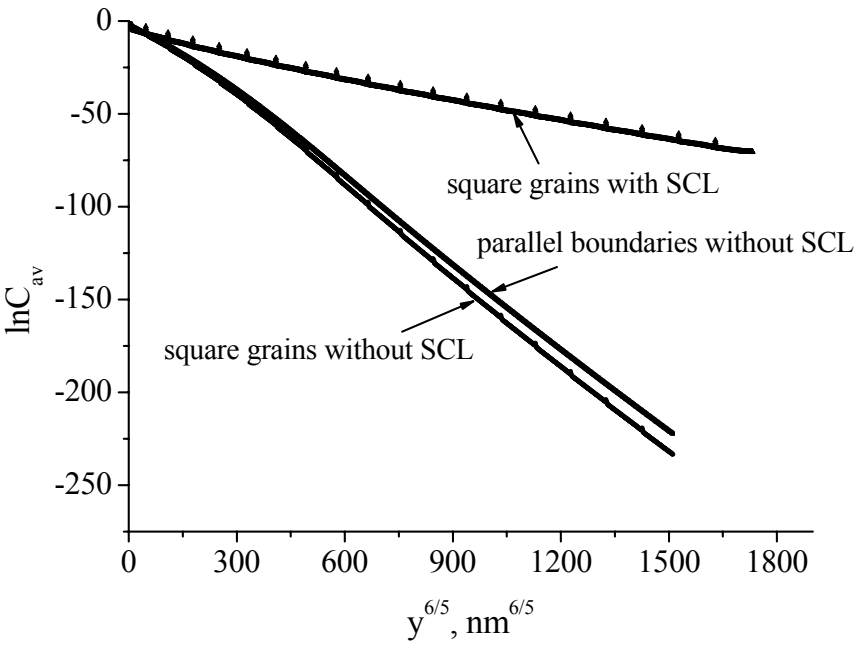

b)

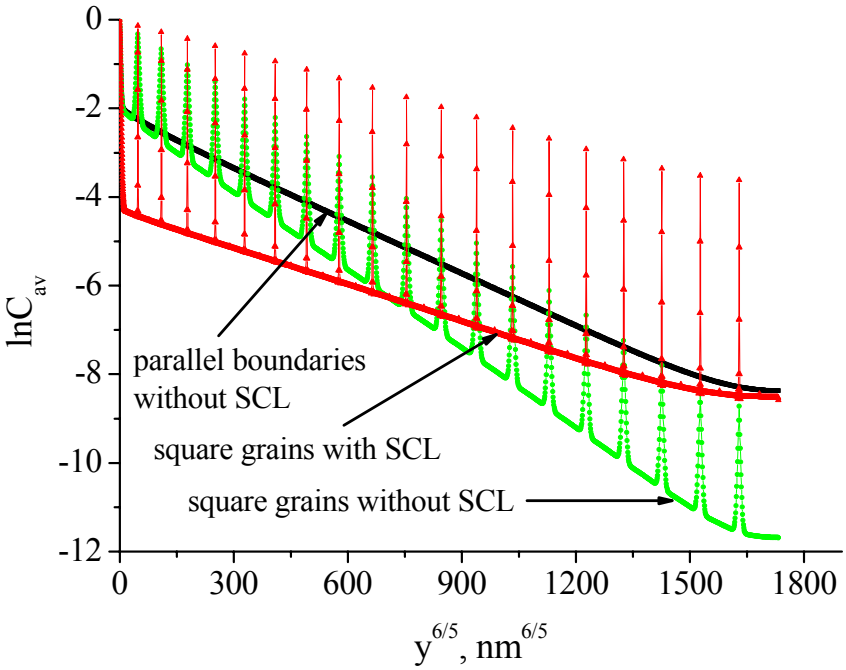

Fig. 5.15 Variation of $\ln C_{av}$ with $y^{6/5}$ calculated for the model of square grains with the GBs surrounded by the blocking SCLs compared with those for the square grains and parallel boundaries without SCLs for $\Lambda = 10^2$ and a) $\Delta = 10^2$, b) $\Delta = 2.2 \cdot 10^4$ at t = 8200 s.

to find $D_{gb,app}$. The error in finding D_{gb} was reduced to 44%, indicating the importance and validity of Eq. (5.3) for SCL problems.

The perpendicular GBs surrounded by the SCLs play a crucial role as it was also discussed in the preceding section. These lead to opposite trends when using the conventional models for the SCL problems and the non-space-charge problems in the B-regime. The concentration distribution is shown in fig. 5.19 for the model of square grains at long t. It is clearly seen that the role of the first grain is very specific. This grain is filled completely by the diffusant, whereas other grains are characterized by much smaller concentrations. The concentration is also enhanced within the GBs. One can expect that the effect of perpendicular GBs with the SCLs is to increase the concentration along the depth, in comparison with the model of parallel boundaries, which is due to deep penetrations. Consequently, the sample can be filled by the diffusant at long t, if each separate grain is filled. However, the perpendicular GBs with the SCLs do not allow the diffusant to proceed further into the next grain. The concentration is drastically reduced due to these GBs (fig. 5.20). An abrupt change of the kinetic regimes occurs along the depth. Again the effect is more pronounced for increasing Λ. Very similar effects due to the blocking SCLs were observed experimentally on different systems [Leo99], [Sou05], and [WanR05]. However, while studying diffusion in polycrystalline materials, it is very difficult to exclude such effects.

At longer t the concentration within the grains increases, and the step between the concentrations in two nearest grains vanishes. It is very well seen in figs. 5.21 and 5.22 for $\Lambda = 10^2$. Nevertheless, the effect of perpendicular GBs is so strong that resolving the problem of SCL by varying t is impossible. In a bicrystal one can estimate at least the role of SCL by plotting $\ln C_{av} = f(y^{6/5})$ even under conditions of the A-regime. In this case the use of Eq. (5.2) is very important, since both the Hart equation and Le Claire's relation yield significant errors. In polycrystals, either high temperature is needed to completely exclude the role of SCL or high gradients are needed to restrict analysis to the process close to the surface, in order to apply the improved procedure for the B-regime discussed in the present study.

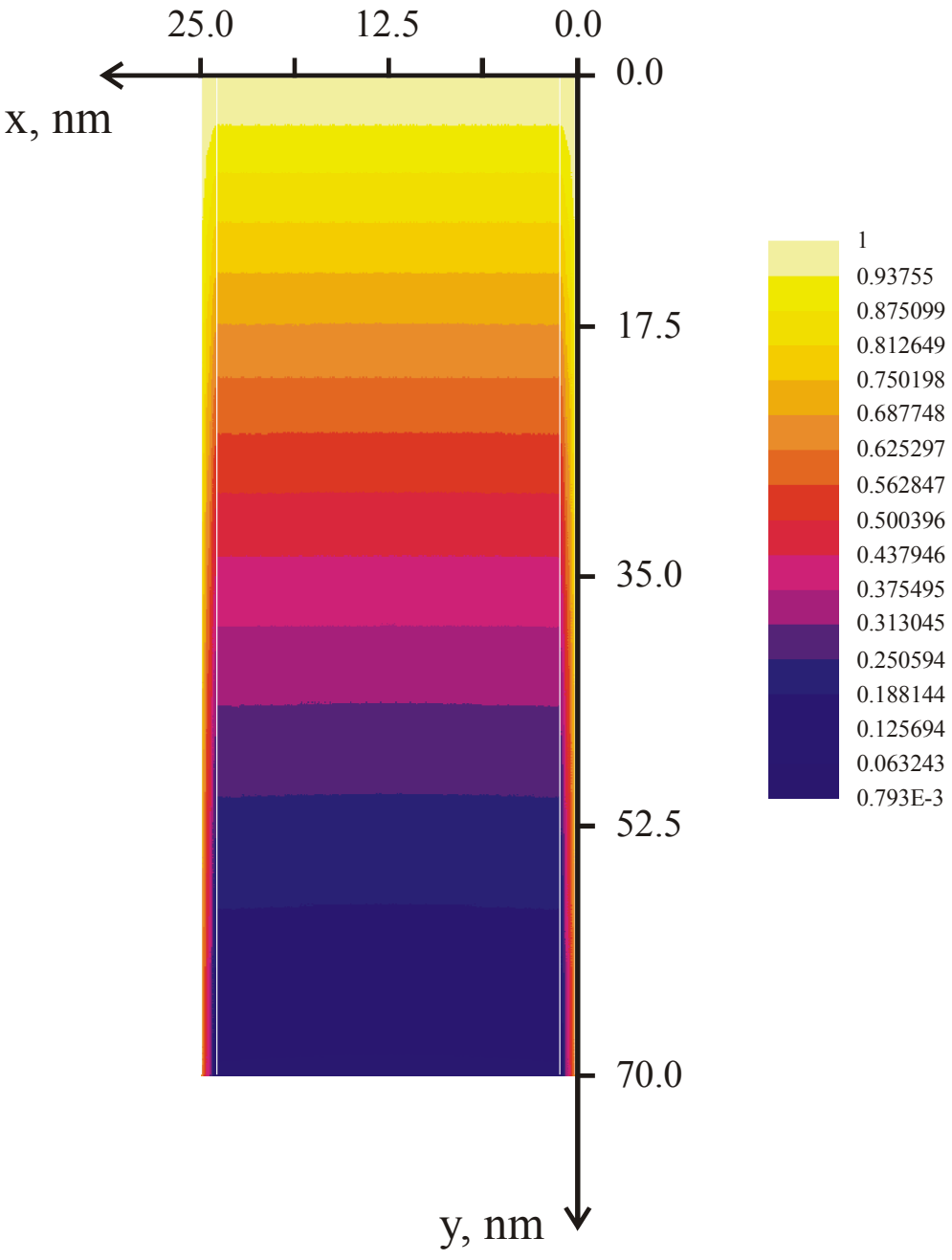

Fig. 5.16 Concentration distribution in the model of parallel boundaries at t = $3 \cdot 10^6$ s. The GBs are used at x = 0.0 and 25.0 nm, whereas white lines correspond to the SCL/grain interface.

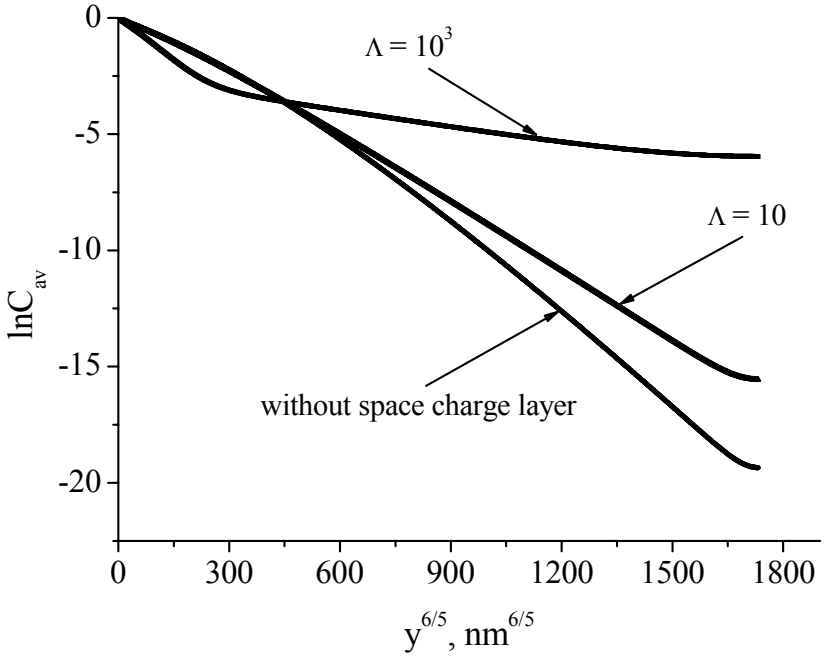

Fig. 5.17 Variation of $\ln C_{av}$ with $y^{6/5}$ calculated for $\Lambda = 10^3$ and $\Lambda = 10$. The diffusion profiles are compared with that without SCL at $t = 3 \cdot 10^6$ s. The ratio Δ is 10^2.

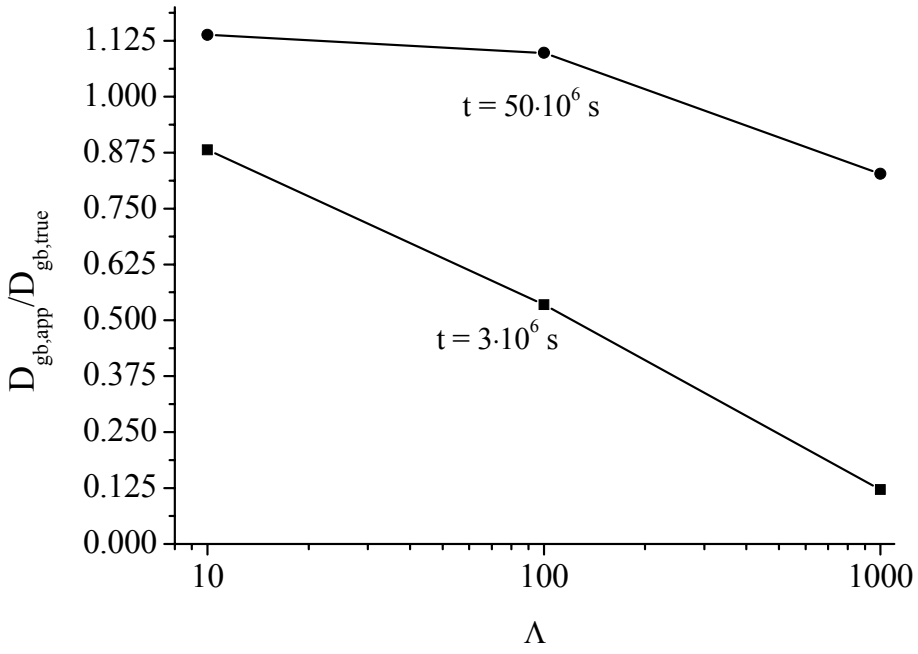

Fig. 5.18 Errors in determining D_{gb} by using conventional Hart's equation.

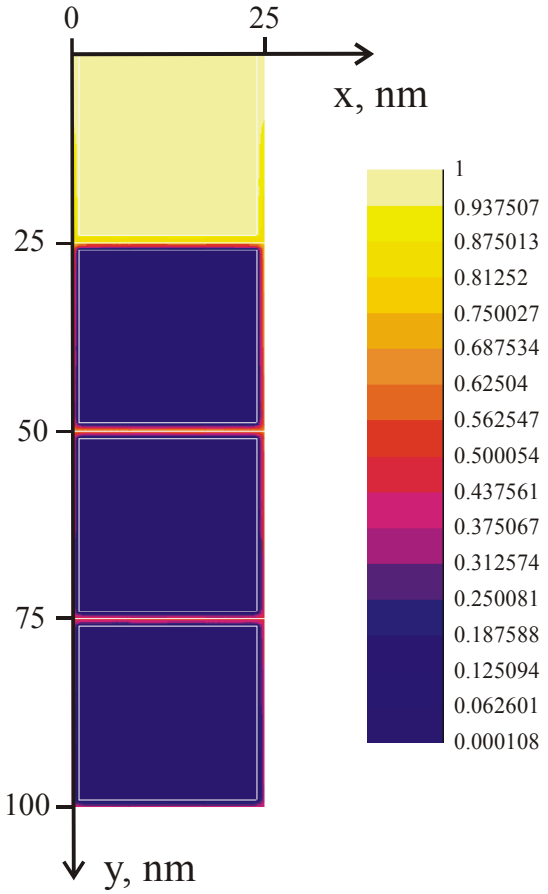

Fig. 5.19 A fragment of the concentration distribution in the model of square grains at $t = 3 \cdot 10^6$ s. The parameters used are the same as in fig. 5.16. The GBs are situated at x = 0.0 and 25.0 nm, y = 25, 50, 75 and 100 nm.

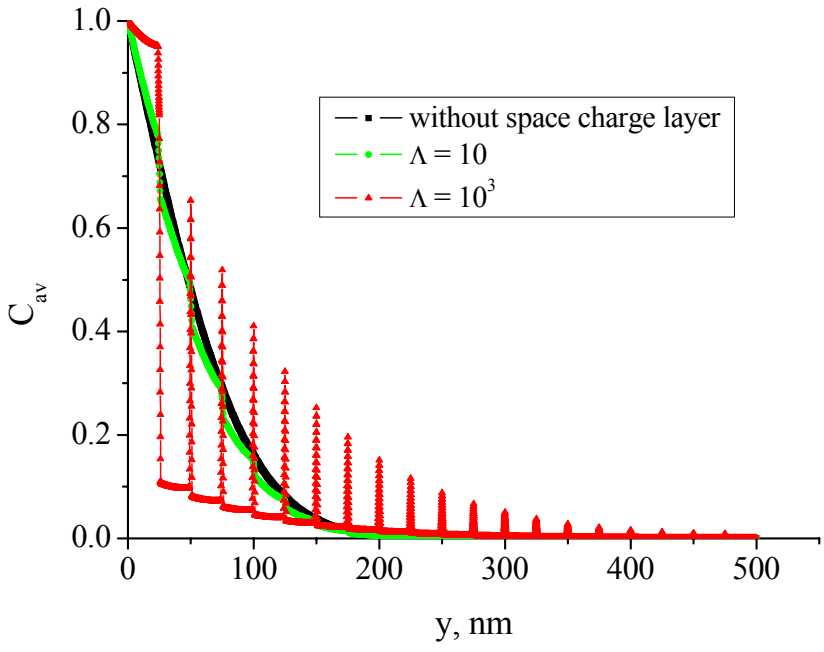

Fig. 5.20 Variation of C_{av} with y calculated at $t = 3 \cdot 10^6$ s for different Λ.

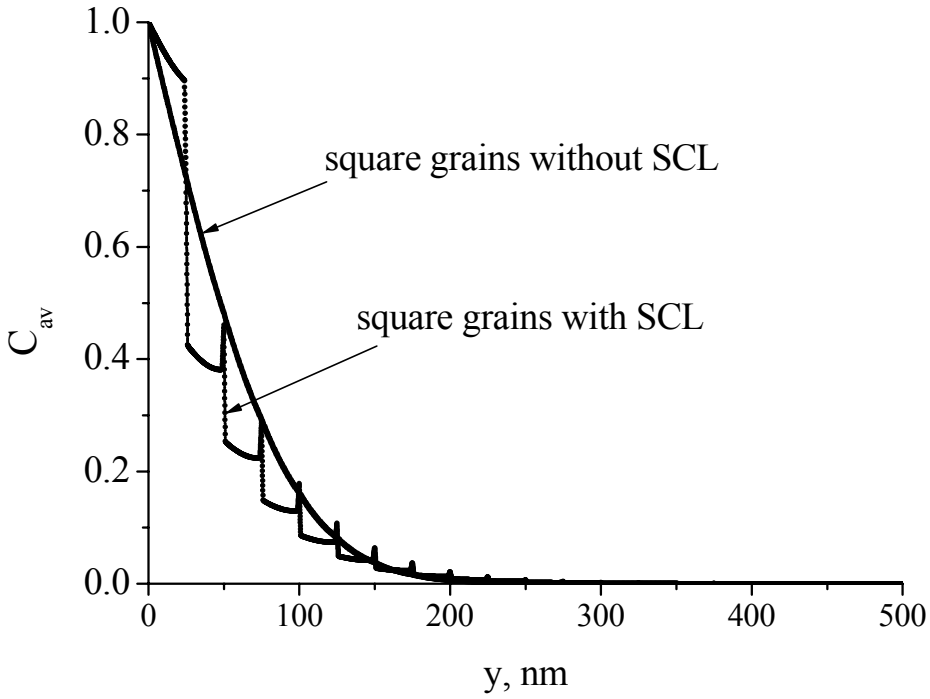

Fig. 5.21 Variation of the diffusion profiles with y calculated for $\Lambda = 10^2$ and $\Delta = 10^2$ at $t = 3 \cdot 10^6$ s are compared with the model without the SCL.

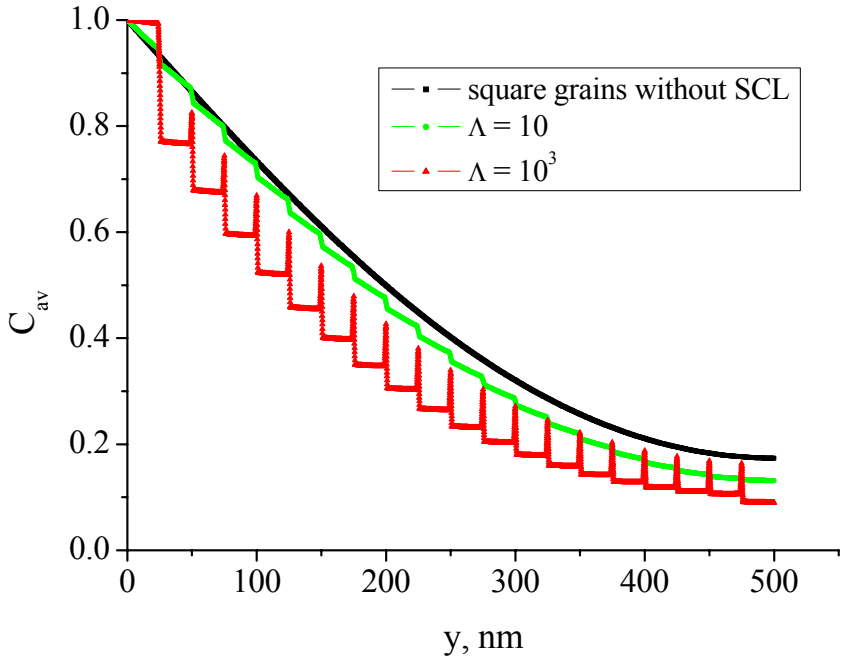

Fig. 5.22 Variation of C_{av} with y calculated for $\Lambda = 10^3$ and $\Lambda = 10$ in the model of square grains. The profiles are compared with that for the model of square grains without SCL for $\Delta = 10^2$ at $t = 50 \cdot 10^6$ s.

Summary

The effects of blocking SCLs were analyzed by simulating the diffusion profiles by means of the finite element approach. The kinetic regimes of type-A and -B were considered and the models of square grains and parallel boundaries applied. A very strong contribution of blocking effects was observed in both the kinetic regimes. This means that space charge effects should definitely be taken into account when deducing D_{gb} from the diffusion profiles measured in ionic materials. In the B-regime D_{gb} is overestimated, and the error increases with the ratio $\Lambda = D_g/D_{scl}$. Importantly, a relation is suggested to find the ratio D_{gb}/D_{scl} from the slopes measured in the B-regime on the basis of equations derived in chapter III. It is proposed how to find D_{gb} by using these new relations. In the A-regime D_{gb} is typically underestimated, and the errors increase with decreasing diffusion time. Again the use of a newly proposed procedure reduced the errors. This confirms the importance of those equations.

Strong concentration drops were observed in microstructure, what is also consistent with the experimental findings. In these cases the main suggestion is to analyze the diffusion profiles close to the surface.